Proceedings of IDETC/CIE 2005
ASME 2005 International Design Engineering Technical Conferences
& Computers and Information in Engineering Conference
September 24-28, 2005, Long Beach, California, USA

DETC2005-85440

CLOSED-FORM NONLINEAR ANALYSIS OF BEAM-BASED FLEXURE MODULES

Shorya Awtar
Precision Engineering Research Group
Massachusetts Institute of Technology
77 Mass Ave 3-470, Cambridge, MA 02139
518-577-5500, shorya@mit.edu

Alexander H. Slocum
Department of Mechanical Engineering
Massachusetts Institute of Technology
77 Mass Ave 3-445, Cambridge, MA 02139
617-253-0012, slocum@mit.edu

ABSTRACT

The simple beam acts as a constraint element when used in flexure mechanisms. Non-linearities arising from the force equilibrium conditions in a beam significantly affect its properties as a constraint element. Consequently, beam-based flexure mechanisms typically suffer from performance tradeoffs in terms of motion range, accuracy and stiffness. This paper presents simple yet accurate approximations that capture this non-linearity and allow for the closed-form analysis of flexure mechanisms of moderate complexity. These general analytical tools enable a designer to parametrically predict key performance parameters of a conceived mechanism such as mobility, over-constraint, stiffness variation, and error motions, without resorting to tedious numerical or computational methods. To illustrate their effectiveness, these approximations are used in deriving the closed-form force-displacement characteristics of several important beam-based flexure modules, and the results are validated using Finite Element Analysis. Variations in the beam shape and flexure module geometry are also considered analytically.

INTRODUCTION

From the perspective of precision machine design [1-4], flexures are essentially constraint elements that rely on material elasticity to allow small yet frictionless motion. The objective of an ideal constraint element is to provide infinite stiffness and zero displacements along it *Degrees of Constraint* (DOC), and allow infinite motion and zero stiffness along its *Degrees of Freedom* (DOF). Despite allowing precise motions, flexures are imperfect constraint devices because neither the range of motion along their DOF, nor the stiffness along their DOC, is infinite. More importantly, the error motions and stiffness values along their DOF and DOC vary with loads and deformations, resulting in fundamental performance tradeoffs in flexure mechanisms [5]. Non-linear effects in the force-displacement characteristics of flexure elements are a primary cause for this behavior. In fact, all the key performance measures such as mobility, over-constraint, stiffness variation, and error motions are affected by these non-linearities. Any undesirable motion in response to a primary motion is considered an error motion, which is classified as a *parasitic error* if it occurs along a DOC and a *cross-axis error* if it occurs along a DOF [5].

Non-linearities in force-displacement characteristics of a flexure beam can arise from one of three sources – material constitutive properties, geometric compatibility, and force equilibrium relations. Flexure beams utilized in precision machine design are generally constructed from metals and operate within the linear elastic limit. But the geometric compatibility relation between the beam's curvature and displacement is an important source of non-linearity. This non-linearity is significant for transverse displacements greater than *0.1L*, and has been thoroughly analyzed in the literature using analytical and numerical methods [6-8]. Simple and accurate parametric approximations based on the pseudo-rigid body method also capture this non-linearity and have proven to be important tools in the design of mechanisms with large displacements [9]. However, it is the non-linearity arising from the force equilibrium expressions that plays a significant role in determining the influence of loads and displacements in one direction on the stiffness properties of other directions, and therefore truly reveals the design tradeoffs in flexure mechanisms. This non-linearity can arise for displacements of the order of the beam's thickness and has been appropriately modeled in the prior literature. Nevertheless, these analyses are too complex for quick design calculations [10], case-specific [11], and require numerical or graphical solution methods [12-13]. This paper suggests the use of simple polynomial

approximations in place of transcendental functions arising from the force equilibrium related non-linearity in beams. These approximations are shown to yield very accurate closed-form force-displacement characteristics of the beam flexure and other beam-based flexure modules, and help quantify the associated performance tradeoffs. Furthermore, the closed-form results enable a physical understanding of flexure mechanism behavior and thus provide important qualitative and quantitative clues for design improvement.

BEAM FLEXURE

Fig.1 illustrates a variable thickness beam with generalized end-forces and end-displacements in a deformed configuration. Displacements and lengths are normalized by the overall beam length L, forces by $E'I_{zz}/L^2$, and moments by $E'I_{zz}/L$. The two end-segments have a uniform thickness t, and the middle section is thick enough to be considered rigid. The symbol E' is used to denote Young's modulus for a state of plane stress, and plate modulus for plane strain. All non-dimensional quantities are represented by lower case letters throughout this discussion.

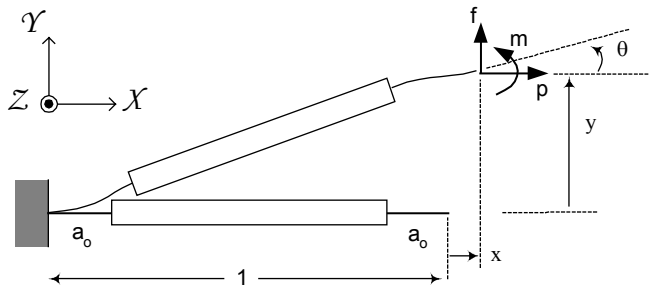

Fig.1 Generalized Beam Flexure

The case of a simple beam ($a_o=1/2$) is first considered. For transverse displacements y and θ less than *0.1*, beam curvature may be linearized by assuming small slopes. If the force equilibrium condition is applied in the deformed configuration of the beam, the axial force p contributes to the bending moments. Solving Euler's equation for the simple beam yields the following well-known results where the tensile axial load $p \triangleq k^2$ [10, 3].

$$f = \frac{k^3 \sinh k}{k\sinh k - 2\cosh k + 2} y + \frac{k^2(1-\cosh k)}{k\sinh k - 2\cosh k + 2}\theta$$
$$m = \frac{k^2(1-\cosh k)}{k\sinh k - 2\cosh k + 2} y + \frac{k^2\cosh k - k\sinh k}{k\sinh k - 2\cosh k + 2}\theta \quad (1)$$

$$y = f\left(\frac{k-\tanh k}{k^3}\right) + m\left(\frac{\cosh k - 1}{k^2\cosh k}\right)$$
$$\theta = f\left(\frac{\cosh k - 1}{k^2\cosh k}\right) + m\left(\frac{\tanh k}{k}\right) \quad (2)$$

$$x = x^e + x^k = \frac{p}{d} - \begin{bmatrix} y & \theta \end{bmatrix}\begin{bmatrix} r_{11} & r_{12} \\ r_{21} & r_{22} \end{bmatrix}\begin{bmatrix} y \\ \theta \end{bmatrix} \quad (3)$$

where,

$$d = \frac{12(1-\nu^2)}{t^2} : \text{Plane Strain} \qquad d = \frac{12}{t^2} : \text{Plane Stress}$$

$$r_{11} = \frac{k^2(\cosh^2 k + \cosh k - 2) - 3k\sinh k(\cosh k - 1)}{2\left(k\sinh k - 2\cosh k + 2\right)^2}$$

$$r_{12} = r_{21} = -\frac{k^2(\cosh k - 1) + k\ \sinh k\ (\cosh k - 1) - 4(\cosh k - 1)^2}{4\left(k\sinh k - 2\cosh k + 2\right)^2}$$

$$r_{22} = \frac{-k^3 + k^2\sinh k(\cosh k + 2) - 2k\ (2\cosh^2 k - \cosh k - 1)}{4k\left(k\sinh k - 2\cosh k + 2\right)^2} + \frac{2\sinh k\ (\cosh k - 1)}{4k\left(k\sinh k - 2\cosh k + 2\right)^2}$$

In the presence of a compressive axial load, expressions analogous to (1)-(3) may be obtained in terms of trigonometric functions instead of hyperbolic functions. The axial displacement x is comprised of two components – a purely elastic component x^e that results due to the elastic stretching of the beam, and a kinematic component x^k that results from the conservation of beam arc-length. The significance of Poisson's ratio, ν, is evident in the normalized elastic axial stiffness d. The kinematic component of the axial displacement may be alternatively stated in terms of the transverse loads, f and m, instead of displacements y and θ. However, it should be recognized that this component fundamentally arises from a condition of geometric constraint, one that requires the beam arc-length to stay constant as it takes a new shape.

Based on the approximations made until this stage, the above results should be accurate to within a few percent of the true behavior of an ideal beam. Although the dependence of transverse stiffness on axial loads and axial stiffness on transverse displacement is evident in expressions (1)-(3), it is practically impossible for a designer to gain any parametric understanding, given the transcendental nature of these expressions. We therefore propose simplifications that are based on an observation that the transverse compliance terms can be accurately approximated by inverse linear or inverse quadratic expressions.

$$C = \begin{bmatrix} \left(\frac{k-\tanh k}{k^3}\right) & \left(\frac{\cosh k - 1}{k^2\cosh k}\right) \\ \left(\frac{\cosh k - 1}{k^2\cosh k}\right) & \left(\frac{\tanh k}{k}\right) \end{bmatrix} \approx \begin{bmatrix} \frac{1}{3\left(1+\frac{2}{5}p\right)} & \frac{1}{2\left(1+\frac{5}{12}p\right)} \\ \frac{1}{2\left(1+\frac{5}{12}p\right)} & \frac{\left(1+\frac{1}{10}p\right)}{\left(1+\frac{17}{40}p+\frac{7}{600}p^2\right)} \end{bmatrix} \quad (4)$$

A comparison of the series expansions of the actual hyperbolic functions and their respective approximations reveals that the series coefficients remain close even for higher order terms. The actual and approximate compliance functions are plotted in Fig.2. It may be verified that the above

approximations result in less than *2.6%* error for relatively large tensile axial forces (*p =10*).

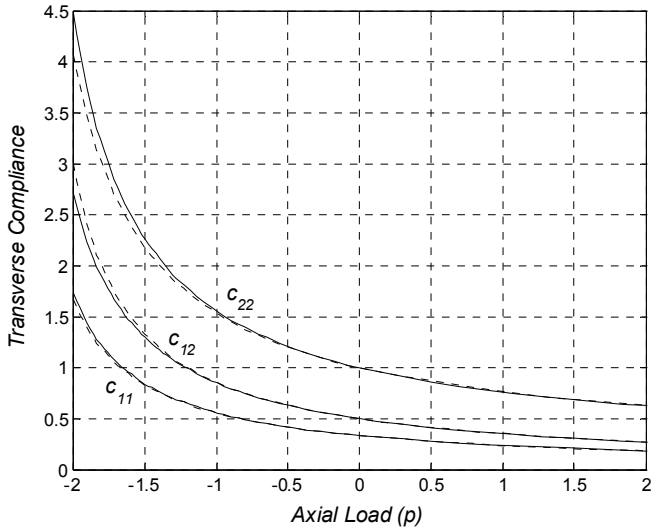

Fig. 2 Actual Compliance Functions (Solid Lines), Approximate Compliance Functions (Dotted Lines)

The fact that some compliance terms can be approximated by inverse linear functions of the axial force implies that the stiffness terms may be approximated simply by linear functions of *p*, which are easily obtained from the series expansion of the hyperbolic stiffness functions.

$$K = \begin{bmatrix} \dfrac{k^3 \sinh k}{k\sinh k - 2\cosh k + 2} & \dfrac{k^2(1-\cosh k)}{k\sinh k - 2\cosh k + 2} \\ \dfrac{k^2(1-\cosh k)}{k\sinh k - 2\cosh k + 2} & \dfrac{k^2\cosh k - k\sinh k}{k\sinh k - 2\cosh k + 2} \end{bmatrix} \approx \begin{bmatrix} 12\left(1+\frac{1}{10}p\right) & -6\left(1+\frac{1}{60}p\right) \\ -6\left(1+\frac{1}{60}p\right) & 4\left(1+\frac{1}{30}p\right) \end{bmatrix} \quad (5)$$

Once again, it should be noted that these expressions are valid not just for small *p*. A series expansion of the stiffness terms shows that the coefficients of the higher order terms are small enough to be neglected even for values of *p* as large as *+/-10*. In this range, the approximation errors are less than *3%*. Similarly, accurate linear approximations can also be made for the coefficients in the geometric constraint relation (3).

$$x^k \approx -\begin{bmatrix} y & \theta \end{bmatrix} \begin{bmatrix} \frac{3}{5}\left(1-\frac{p}{420}\right) & -\frac{1}{20}\left(1-\frac{p}{70}\right) \\ -\frac{1}{20}\left(1-\frac{p}{70}\right) & \frac{1}{15}\left(1-\frac{11p}{420}\right) \end{bmatrix} \begin{bmatrix} y \\ \theta \end{bmatrix} \quad (6)$$

While this excellent match is mathematically a coincidence, its advantages are far-fetched in terms of revealing the key physical attributes of a beam flexure. Although shown for the tensile axial load case, all of the above approximations hold valid for the compressive case as well. Summarizing the results in a general format,

$$\begin{bmatrix} f \\ m \end{bmatrix} = \begin{bmatrix} a & c \\ c & b \end{bmatrix} \begin{bmatrix} y \\ \theta \end{bmatrix} + p \begin{bmatrix} e & h \\ h & g \end{bmatrix} \begin{bmatrix} y \\ \theta \end{bmatrix} \quad (7)$$

$$x = \frac{1}{d}p + \begin{bmatrix} y & \theta \end{bmatrix} \begin{bmatrix} i & k \\ k & j \end{bmatrix} \begin{bmatrix} y \\ \theta \end{bmatrix} + p \begin{bmatrix} y & \theta \end{bmatrix} \begin{bmatrix} r & q \\ q & s \end{bmatrix} \begin{bmatrix} y \\ \theta \end{bmatrix} \quad (8)$$

The coefficients *a*, *b*, *c*, *e*, *g*, *h*, *i*, *j*, *k*, *q*, *r* and *s* are all non-dimensional numbers that are characteristic of the beam shape, and assume the following values for a simple beam with uniform thickness.

a	12	*e*	1.2	*i*	-0.6	*r*	1/700
b	4	*g*	2/15	*j*	-1/15	*s*	11/6300
c	-6	*h*	-0.1	*k*	1/20	*q*	-1/1400

These symbols are used throughout this paper to represent the indicated numerical values. In general, these coefficients are functionals of the beam's spatial thickness function *t(X)*. A quantification of these coefficients in terms of the beam shape provides the basis for a sensitivity analysis and shape optimization. Shape variations of the kind considered in Fig.1 are discussed in further detail, later in this section.

The maximum estimated error in the analysis so far is of the order of *5-6%* for transverse displacements within *+/-0.1* and axial loads within *+/-10*. Unlike the linear analysis, expressions (7)-(8) clearly express the role of the normalized axial load *p* in the force-displacement properties of the beam in a simple matrix format. The two components of transverse stiffness, commonly referred to as the elastic stiffness matrix and the geometric stiffness matrix, are also clearly quantified in expression (7). The accuracy of these derivations may be further verified using known cases of beam buckling. Buckling limit corresponds to the compressive load at which the transverse stiffness of a beam becomes zero. Using this definition and expression (4) for a fixed-free beam, one can estimate the buckling load to be $p_{crit} = -2.5$, which is less than *1.3%* off from the classical beam buckling prediction of $p_{crit} = -\pi^2/4$. Similarly, the buckling load for a beam with zero end slopes is predicted to be *-10* using expression (5), as compared to $-\pi^2$ derived using the classical theory. Many other non-trivial results can now be easily derived from the proposed simplified expressions, using appropriate boundary conditions. For example, in the presence of an axial load *p,* the ratio between *m* and *f* required to ensure zero beam-end rotation is given by $-\left(1+\frac{1}{60}p\right)/2\left(1+\frac{1}{10}p\right)$, which determines the center of stiffness of the beam. An example that illustrates a design tradeoff is that of a clamped-clamped beam of length *2L* transversely loaded in the center. While symmetry ensures perfect straight-line motion along the *y* DOF, and no error motions along the *x* DOC, it also results in a non-linear stiffening effect along the DOF given by $f = 2(a - i\,d\,e\,y^2)y$, which significantly limits the range of desirable motion. This non-linear stiffness behavior can be derived in a few steps from

expressions (7)-(8), whereas the conventional methods are considerably more time-consuming.

Of much interest is the change in axial stiffness in the presence of a transverse displacement as quantified in expression (8). It may be seen that the kinematic component defined earlier may be further separated into a purely kinematic component, and an *elastokinematic* component. The latter is named so because of its dependence on the axial force as well as the kinematic requirement of constant beam arc-length. This component essentially captures the effect of the change in the beam's deformed shape due to the contribution of the axial force to the bending moments. Along with the purely elastic component, this term also contributes to the axial compliance. This is important in flexure design because the axial compliance of a beam flexure determines the quality of its DOC, which in turn influences static as well as dynamic performance. Thus, the range of motion along DOF is limited to ensure an acceptably small stiffness reduction along the DOC.

Next, we consider the relatively generalized beam of Fig. 1. The non-linear force-displacement characteristics for this beam geometry may be obtained by treating the two end-segments as simple beams, and using the prior results of this section. As the dimension a_o becomes smaller, Bernoulli's assumptions are obviously compromised and correction factors should be used for an accurate prediction. Nevertheless, the present treatment illustrates the effect of a beam's geometry variation on the nature of its force-displacement characteristics.

$$\begin{bmatrix} f \\ m \end{bmatrix} \approx \frac{3}{a_o\left(4a_o^2 - 6a_o + 3\right)} \cdot \begin{bmatrix} 2+\left(a_o - \frac{17}{20}a_o^2\right)p & -1-\left(\frac{13}{40}a_o^2 - \frac{41}{120}a_o^3\right)p \\ -1-\left(\frac{13}{40}a_o^2 - \frac{41}{120}a_o^3\right)p & 1-a_o+\frac{2}{3}a_o^2+\left(-\frac{1}{3}a_o^3+\frac{13}{40}a_o^2\right)p \end{bmatrix} \begin{bmatrix} y \\ \theta \end{bmatrix} \tag{9}$$

This approximation is valid for all values of a_o in the absence of an axial load, and only for small values of a_o (*~0.1*) in the presence axial loads. It is noteworthy that this expression is of the same matrix equation format as expression (7). As expected, reducing the length of the end-segments increases the transverse stiffness values of the beam. Similarly, an expression analogous to (8) can be derived for the pertinent beam geometry. For brevity, only the purely kinematic term associated with y^2, which is the most important, is stated.

$$i = -\left(\frac{1-\frac{10}{3}a_o+4a_o^2-\frac{8}{5}a_o^3}{2-8a_o+\frac{40}{3}a_o^2-\frac{32}{3}a_o^3+\frac{32}{9}a_o^4}\right) \tag{10}$$

When a_o*=1/2*, the above expression yields y*= -0.6*, which is the expected result for a simple beam. For values of a_o approaching zero, the above coefficient becomes *–1/2* and all other elastic, kinematic and elastokinematic terms reduce to zero, exactly as expected of a hinged-hinged rigid link. Beams with even further generalized geometries such as continuously varying thickness may be similarly modeled. This particular example shows that despite variations in the beam shape, the dependence of transverse stiffness on axial load and axial stiffness on transverse displacements are still governed by the general expressions (7) and (8), and only the non-dimensional numerical coefficients change. Although, all the subsequent flexure modules considered in this paper are based on the simple beam, other beam shapes may be treated with equal ease.

PARALLELOGRAM FLEXURE AND VARIATIONS

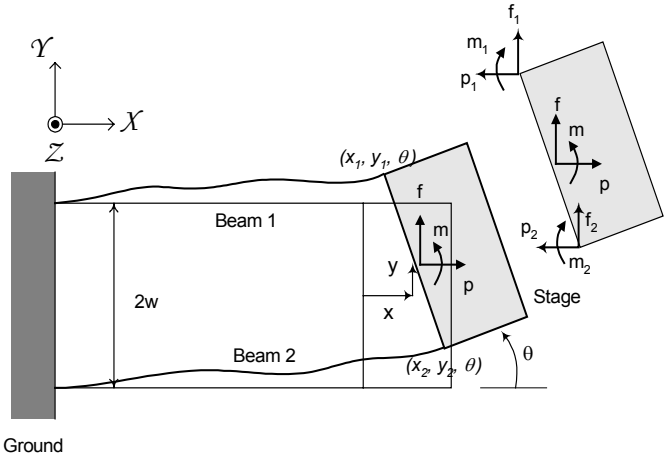

Fig. 3 Parallelogram Flexure and Stage Free Body Diagram

The beam-based parallelogram flexure is frequently employed to provide an approximate straight-line motion. In this case, the y displacement represents a DOF, and x and θ represent DOC. The stage connecting the two beams in a parallelogram flexure, illustrated in Fig. 3, is assumed rigid. The two beams are initially treated identical, and therefore loads and displacements can be normalized with respect to the properties of either beam. Linear analysis of the parallelogram flexure module, along with the kinematic requirement of constant beam arc-length, yields the following standard results [3].

$$\begin{bmatrix} f \\ m \end{bmatrix} = 2\begin{bmatrix} a & c \\ c & w^2d+b \end{bmatrix}\begin{bmatrix} y \\ \theta \end{bmatrix} \approx 2\begin{bmatrix} a & c \\ c & w^2d \end{bmatrix}\begin{bmatrix} y \\ \theta \end{bmatrix}$$
$$x = \frac{p}{2d} + iy^2 \tag{11}$$

However, our objective here is to determine the true non-linear force-displacement characteristics of the parallelogram flexure. Based on the linear analysis, stage rotation θ is of the order of 10^{-5} radians for typical dimensions and a y displacement of *0.1*. This observation allows us to drop out the higher order terms of θ in several places. Conditions of geometric compatibility yield,

$$x = \frac{(x_1^e + x_2^e)}{2} + \frac{(x_1^k + x_2^k)}{2} \triangleq x^e + x^k$$
$$w\theta = \frac{(x_1^e - x_2^e)}{2} + \frac{(x_1^k - x_2^k)}{2} \tag{12}$$

Force equilibrium conditions are derived from the Free Body Diagram of the stage in Fig. 3. While force equilibrium is applied in a deformed configuration to capture non-linear effects, the contribution of θ is negligible.

$$p_1 + p_2 = p \quad ; \quad f_1 + f_2 = f \quad ; \quad m_1 + m_2 + (p_2 - p_1)w = m \tag{13}$$

Force displacement results (7)-(8) are be applied for each beam and yield,

$$\begin{aligned} f &= f_1 + f_2 = (2a + pe)y + (2c + ph)\theta \\ m_1 + m_2 &= (2c + ph)y + (2b + pg)\theta \end{aligned} \tag{14}$$

Unlike in a linear analysis, it is important to recognize that neither f_1 equals f_2 and nor m_1 equals m_2, despite the fact that the transverse displacements for the two beams are constrained to be the same. This is due to the different values of axial forces p_1 and p_2, which result in unequal transverse stiffness changes in the two beams. Using equations (12)-(14), one can now solve the force-displacement relationships of the parallelogram flexure.

$$\begin{aligned} \theta &= \left\{ \frac{1}{d} + \begin{bmatrix} y & \theta \end{bmatrix} \begin{bmatrix} r & q \\ q & s \end{bmatrix} \begin{bmatrix} y \\ \theta \end{bmatrix} \right\} \cdot \\ &\quad \left\{ \frac{m - (2c + ph)y + (2b + pg)\theta}{2w^2} \right\} \\ x^e &= \frac{1}{2d}(p_1 + p_2) = \frac{p}{2d} \\ x^k &= \begin{bmatrix} y & \theta \end{bmatrix} \begin{bmatrix} i & k \\ k & j \end{bmatrix} \begin{bmatrix} y \\ \theta \end{bmatrix} + \frac{p}{2} \begin{bmatrix} y & \theta \end{bmatrix} \begin{bmatrix} r & q \\ q & s \end{bmatrix} \begin{bmatrix} y \\ \theta \end{bmatrix} \\ y &= \frac{f - (2c + ph)\theta}{(2a + pe)} \end{aligned} \tag{15}$$

The first term in the expression for θ represents the consequence of elastic contraction and stretching of the top and bottom beams, respectively. The second term, which is rarely accounted for in the literature, is the consequence of the elastokinematic effect explained in the previous section. Since the axial loads on the two beams are different, apart from resulting in different elastic deflections of the two beams, they also cause slightly different beam shapes and therefore different elastokinematic deflections. Because of its linear dependence on the axial load and quadratic dependence on the transverse displacement, the elastokinematic effect contributes a non-linear component to the stage rotation. The purely kinematic part of the axial deflection of the beams is independent of the axial force and depends only on the tip displacements, and therefore does not contribute to θ. The axial displacement of the stage is comprise of a purely elastic component, a purely kinematic component and an elastokinematic component. Solving and simplifying equations (15), displacements are obtained in terms of the loads.

$$\theta = \frac{\left(4a^2 + 4pea + p^2e^2 + f^2dr\right)\left(2ma - 2fc + p(me - fh)\right)}{2w^2d(2a + ep)^3} \tag{16}$$

$$y = \frac{f - (2c + ph)\theta}{(2a + pe)} \approx \frac{f}{(2a + pe)} \tag{17}$$

$$x \approx \frac{p}{2d} + y^2 i + \frac{p}{2} y^2 r \tag{18}$$

For nominal dimensions of $t=1/60$ and $w=1/3$, stage rotation predictions based on the linear analysis, non-linear analysis for different axial loads, and Finite Element Analysis are plotted in Fig.4. The center of stiffness of the parallelogram module, i.e., the location on the stage where a transverse load may be applied without causing any stage rotation, is given by the ratio between m and f that makes the stage rotation zero. This ratio is easily calculated from (16) to be $(2c + ph)/(2a + pe)$ and is equal to -0.5 in the absence of an axial load, which agrees with common knowledge.

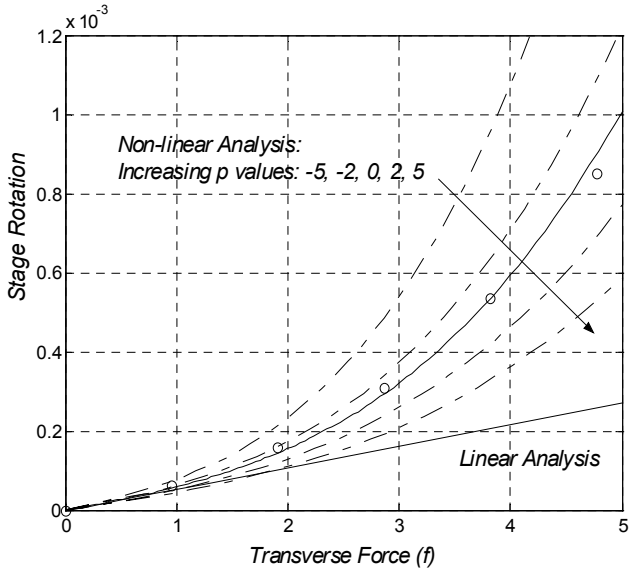

Fig. 4 Parallelogram Stage Rotation: Closed-form Linear and Non-linear Analyses (Lines), FEA (Circles)

Expression (17) describes the transverse force displacement behavior of the parallelogram flexure, which is plotted in Fig. 5. As expected, the transverse stiffness has a linear dependence on the axial load, and approaches zero for $p=-20$, which physically corresponds to the condition for buckling. In this expression, the θ dependence, and therefore the m dependence, has been dropped since it is several orders smaller than y. However, it should be recognized that since θ is dependent on f, reciprocity requires y to be dependent on m. This dependence is important only in specific cases, for example, when the transverse end load is a pure moment.

The axial force-displacement characteristics are given by expression (18), which quantifies the dependence of axial compliance on transverse displacements. Axial stiffness drops quadratically with y and the rate of this drop depends on the coefficient r, which is $1/700$ for a simple beam. For a typical case when $t=1/60$, the axial stiffness reduces by about *13%* for a transverse displacement of *0.05*, as shown in Fig.6. This

characteristic of the parallelogram flexure module represents the quality of its DOC, and determines its suitability as a building block in flexure mechanisms. This module may be mirrored about the motion stage, and the resulting symmetry eliminates any x or θ error motions in response to a primary y motion, and improves the axial stiffness. Nevertheless, this attempt to improve the quality of DOC results in a non-linear stiffness in the DOF direction, leading to over-constraint.

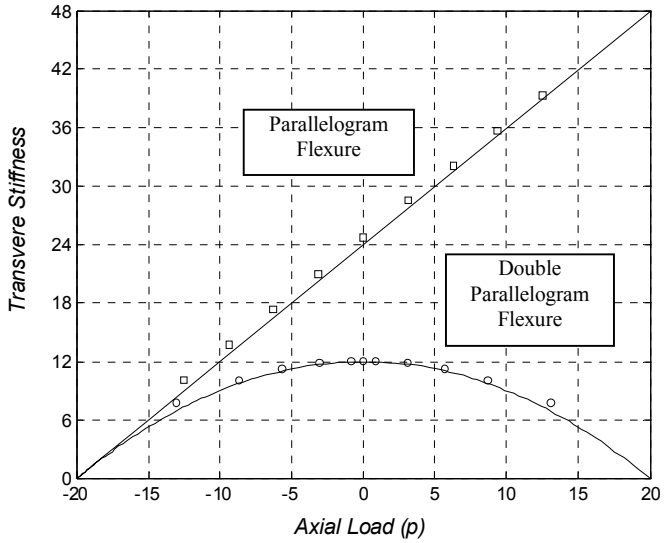

Fig. 5 Transverse Stiffness of Parallelogram and Double Parallelogram Flexures: Closed-form Analysis (Solid Lines), FEA (Circles, Squares)

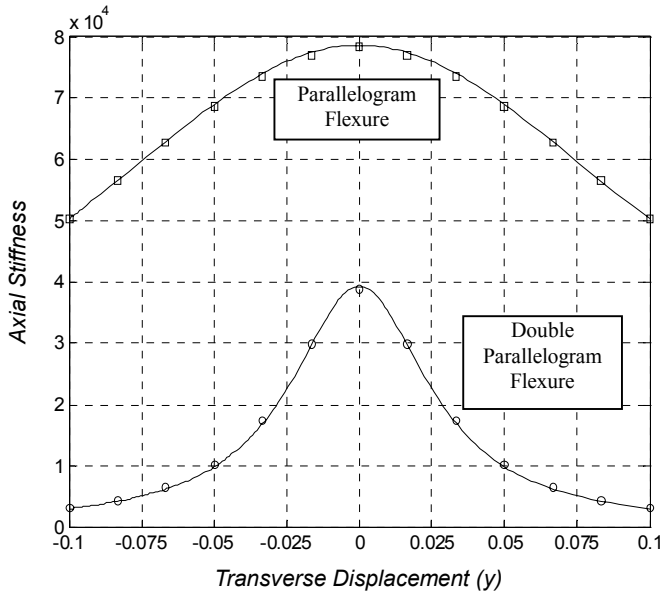

Fig. 6 Axial Stiffness of Parallelogram and Double Parallelogram Flexures: Closed-form Analysis (Solid Lines), FEA (Circles, Squares)

Furthermore, a sensitivity analysis may be performed to determine the effect of differences between the two beams in terms of material, shape, thickness, length or separation. For the sake of illustration, a parallelogram flexure with beams of unequal lengths, L_1 and L_2, is considered. L_1 is used as the characteristic length in the mechanism and error metric Δ is defined to be $(1–L_2/L_1)$. Force-displacement relationships for Beam 1 remain the same as earlier (7)-(8), whereas those for Beam 2 change as follows for small Δ.

$$\begin{bmatrix} f_2 \\ m_2 \end{bmatrix} = \begin{bmatrix} (1+3\Delta)a & (1+2\Delta)c \\ (1+2\Delta)c & (1+\Delta)b \end{bmatrix} \begin{bmatrix} y \\ \theta \end{bmatrix} + p_2 \begin{bmatrix} (1+\Delta)e & h \\ h & (1-\Delta)g \end{bmatrix} \begin{bmatrix} y \\ \theta \end{bmatrix}$$

$$x_2^e = \frac{(1-\Delta)}{d} p_2$$

$$x_2^k = \begin{bmatrix} y & \theta \end{bmatrix} \begin{bmatrix} (1+\Delta)i & k \\ k & (1-\Delta)j \end{bmatrix} \begin{bmatrix} y \\ \theta \end{bmatrix} + p_2 \begin{bmatrix} y & \theta \end{bmatrix} \begin{bmatrix} (1-\Delta)r & (1-2\Delta)q \\ (1-2\Delta)q & (1-3\Delta)s \end{bmatrix} \begin{bmatrix} y \\ \theta \end{bmatrix} \tag{19}$$

Conditions of geometric compatibility (12) and force equilibrium (13) remain the same. These equations may be solved simultaneously, and for the specific case of $m=p=0$ result in the following stage rotation.

$$\theta = \frac{x_2 - x_1}{2w} \approx -\frac{(c+\Delta)(2-\Delta)}{2w^2}\left(\frac{y}{d} + ry^3\right) + \frac{iy^2}{2w}\Delta \tag{20}$$

Setting $\Delta=0$ obviously reduces this to the stage rotation for the ideal case. It may be noticed that unequal beam lengths result in an additional term in the stage rotation, which has a quadratic dependence on the transverse displacement. This is due to the purely kinematic effect in the beams that was cancelled out earlier because of the identical geometric properties of the two beams.

Another important variation of the parallelogram flexure is the tilted-beam flexure in which the two beams are not perfectly parallel, as shown in Fig.7. This may result due to poor manufacturing and assembly tolerances, or because of an intentional design to achieve a remote center of rotation at C_1. Assuming a symmetric geometry and repeating the analysis as in the previous two cases, the following non-linear force-displacement results are obtained for this tilted-beam flexure configuration.

$$\theta \approx -\frac{y \tan\alpha}{w} \approx -\frac{y\alpha}{w} \tag{21}$$

$$y \approx \frac{\left(f - m\frac{\alpha}{w}\right)\cos\alpha}{\left(2a - \frac{4c}{w}\alpha + \frac{2b}{w^2}\alpha^2 - 2a\alpha^2 + 2\frac{c}{w}\alpha^3\right) + \left(e - 2\frac{h}{w}\alpha\right)p} \tag{22}$$

$$x \approx \frac{p}{2d\cos^2\alpha} + \frac{y^2}{\cos^3\alpha}\left[\left(i - 2k\frac{\alpha}{w} + j\frac{\alpha^2}{w^2}\right) + \left(r - 2q\frac{\alpha}{w} + s\frac{\alpha^2}{w^2}\right)\frac{p}{2\cos\alpha}\right]$$

$$\triangleq \frac{p}{2d\cos^2\alpha} + \frac{y^2\left(\bar{i} + \bar{r}\frac{p}{2}\right)}{\cos^3\alpha} \tag{23}$$

These derivations are made assuming small but non-zero values of α *(~ 0.1)*. The most important observation here is that unlike the ideal parallelogram flexure, the stage rotation θ here has a dominant kinematic dependence on the primary motion *y*, irrespective of the loads. This implies that the motion stage has an approximate virtual center of rotation located at C_1, which is expected. Quantitative results (20) and (21), regarding the stage rotation, are in perfect agreement with the empirical observations made in the prior literature [14]. The primary motion compliance in the tilted-beam flexure is a function of α, and the primary motion itself has a dependence on the end-moment *m*, as shown by expression (22). The axial displacement in this case is very similar in nature to the axial displacement of the parallelogram flexure, except in this case the stage rotation is not negligible and therefore contributes to all the kinematic terms. Expression (23) shows that the elastic, kinematic as well as elastokinematic compliance terms increase due to the tilted beam geometry, thus compromising the quality of the *x* DOC. The tilted-beam flexure is clearly not a good replacement of the parallelogram flexure if straight-line motion is desired, but is important as a virtual frictionless pivot mechanism.

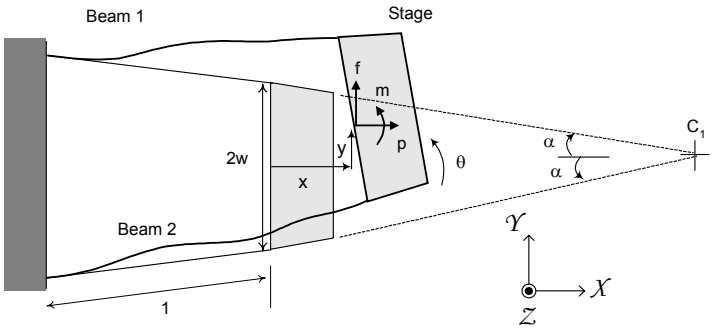

Fig.7 Tilted-beam Flexure

DOUBLE PARALLELOGRAM FLEXURE AND VARIATIONS

The results of the previous section are easily extended to a double parallelogram flexure, illustrated in Fig. 8. The two rigid stages are referred to as the primary and secondary stages, as indicated. Loads *f*, *m* and *p* are applied at the primary stage. The two parallelograms are treated as identical, except for the beam spacing, w_1 and w_2. A linear analysis yields the following force-displacement characteristics.

$$\begin{bmatrix} f \\ m \end{bmatrix} = \begin{bmatrix} a & -a/2 \\ -a/2 & \dfrac{2w_1^2 w_2^2 d}{w_1^2 + w_2^2} \end{bmatrix} \begin{bmatrix} y \\ \theta \end{bmatrix} \qquad \text{and} \qquad x = \frac{p}{d} \tag{24}$$

For a non-linear analysis, force-displacement results obtained in the previous section are applied to each of the constituent parallelograms. Geometric compatibility and force equilibrium conditions are easily obtained from Fig. 8. Solving these simultaneously leads to the following results.

$$y \approx \frac{4af}{(2a)^2 - (ep)^2} \tag{25}$$

$$\theta = \begin{bmatrix} fn_1(p) & fn_2(p) & fn_3(p) & fn_4(p) \end{bmatrix} \begin{bmatrix} f \\ m \\ f^3 \\ mf^2 \end{bmatrix} \tag{26}$$

where,

$$fn_1(p) = \frac{\begin{bmatrix} 1 & p & p^2 \end{bmatrix} \begin{bmatrix} 4a^2w_2^2 + 4ac(w_2^2 - w_1^2) \\ -2ah(w_2^2 + w_1^2) + 2ce(w_2^2 + w_1^2) - 2aw_2^2 \\ he(w_1^2 - w_2^2) + w_2^2 e(1-e) \end{bmatrix}}{2dw_1^2 w_2^2 \left((2a)^2 - (ep)^2\right)}$$

$$fn_2(p) = \frac{(w_2^2 + w_1^2)}{2dw_1^2 w_2^2}$$

$$fn_3(p) = \frac{r\begin{bmatrix} 1 & p & p^2 & p^3 & p^4 \end{bmatrix}}{2w_1^2 w_2^2 \left((2a)^2 - (ep)^2\right)^3} \cdot \begin{bmatrix} 16a^4w_2^2 + 16a^3c(w_2^2 - w_1^2) \\ -8a^3h(w_2^2 + w_1^2) + 24a^2ce(w_2^2 + w_1^2) - 8a^3w_2^2(1-2e) \\ 12ace^2(w_2^2 - w_1^2) + 12a^2he(w_1^2 - w_2^2) - 4a^2w_2^2e \\ -6ahe^2(w_2^2 + w_1^2) + 2ce^3(w_2^2 + w_1^2) + 2aw_2^2e^2(1-2e) \\ he^3(w_1^2 - w_2^2) + w_2^2e^3(1-e) \end{bmatrix}$$

$$fn_4(p) = \frac{r\begin{bmatrix} 1 & p & p^2 \end{bmatrix} \begin{bmatrix} 4a^2(w_2^2 + w_1^2) \\ 4ae(w_2^2 - w_1^2) \\ e^2(w_2^2 + w_1^2) \end{bmatrix}}{2w_1^2 w_2^2 \left((2a)^2 - (ep)^2\right)^2}$$

$$x_1 = -\frac{p}{2d} + y_1^2\left(i - \frac{pr}{2}\right) \quad ; \quad x + x_1 = \frac{p}{2d} + (y - y_1)^2\left(i + \frac{pr}{2}\right)$$

$$\Rightarrow x = \frac{p}{d} + py^2 \frac{r\left[(2a)^2 + (ep)^2\right] - 8aei}{(4a)^2} \tag{27}$$

Expression (25) describes the primary motion behavior and does not include the weak dependence on *m*. Similar to the parallelogram flexure, *y* displacement represents a DOF while *x* and θ displacements represent DOC. However, in this case, stiffness in the DOF direction decreases quadratically with an axial load. This quadratic dependence is a consequence of the fact that one parallelogram is always in tension while the other is in compression, irrespective of the direction of the axial load. A comparison of the transverse stiffness values for a parallelogram and a double parallelogram flexure with the same characteristic length is shown in Fig.5.

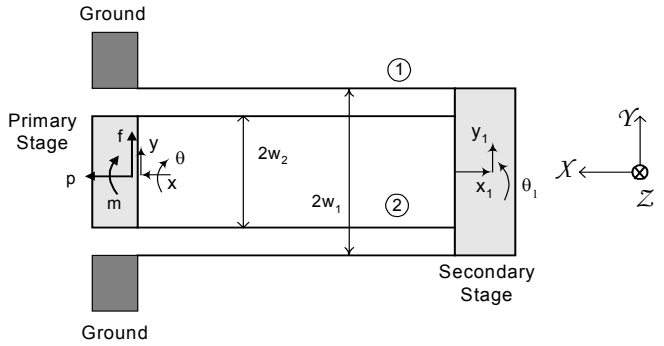

Fig.8 Double Parallelogram Flexure

Expression (26) for primary stage rotation θ of a double parallelogram flexure is similar in structure to the parallelogram stage rotation, but its non-linear dependence on the axial load p is more complex. In the absence of a moment load, the primary stage rotation θ is plotted against the transverse force f, for various axial loads, in Fig.9. These results are obtained for a typical geometry of $t=1/60$, $w_1=0.5$ and $w_2=0.3$. It may be seen that the overall stiffness in general and the non-linear contribution in particular increases with axial forces. Furthermore, the change in the θ-f relationship with axial forces is relatively less as compared to the parallelogram flexure because for a given axial load, one of the constituent parallelograms is in tension and the other is in compression. The increase in stiffness of the former is somewhat compensated by the reduction in stiffness of the latter, thereby reducing the overall dependence on axial loads.

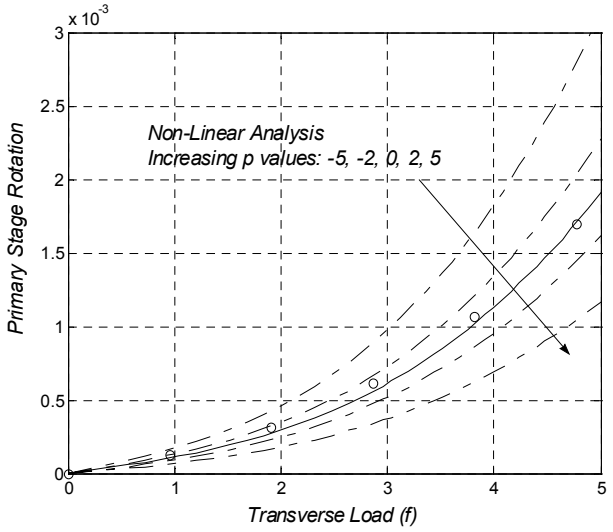

Fig.9 Double Parallelogram Stage Rotation: Closed-form Linear and Non-linear Analyses (Lines), FEA (Circles)

The center of stiffness for the double parallelogram flexure may be analytically obtained from expression (26). Despite the non-linear dependence of θ on transverse forces, the m/f ratio required to keep the primary stage rotation zero, in the absence of an axial load, is given by $-\frac{w_2^2(a+c)-w_1^2 c}{(w_2^2+w_1^2)a}=-\frac{1}{2}$, which predictably changes in the presence of an axial force. Nevertheless, parasitic error motion θ may be eliminated by appropriate locating the end force f.

The non-dimensional axial displacement expression (27) reveals a purely elastic term as well as an elastokinematic term, but no purely kinematic term. The purely kinematic term gets absorbed by the secondary stage due to geometric reversal. While the purely elastic term is as expected, the elastokinematic term is significantly different from the parallelogram flexure, and is not immediately obvious. The axial compliance may be further simplified as follows.

$$\frac{\partial x}{\partial p}\approx\frac{1}{d}+\frac{y^2}{2}\left(\frac{r}{2}-\frac{ei}{a}\right) \tag{28}$$

Of the two factors that contribute elastokinematic terms, $r/2$ and ei/a, the latter being two orders larger than the former dictates the axial compliance. This ei/a contribution does not exist in the parallelogram flexure, and is a consequence of the double parallelogram geometry. When a y displacement is imposed on the primary stage, the transverse stiffness values for the two parallelograms are equal if the there is no axial load, and therefore y is equally distributed between the two. Referring to Fig. 8, as a tensile axial load is applied, the transverse stiffness of parallelogram 1 decreases and that of parallelogram 2 increases by the same amount, which results in a proportionate redistribution of y between the two. Since the kinematic axial displacement of each parallelogram has a quadratic dependence on its respective transverse displacement, the axial displacement of parallelogram 1 exceeds that of parallelogram 2. This difference results in the unexpectedly large elastokinematic component in the axial displacement and compliance. If the axial load is compressive in nature, the scenario remains the same, except that the two parallelograms switch roles.

For the geometry considered earlier, the axial stiffness of a double parallelogram flexure is plotted against its transverse displacement y in Fig.6, which shows that the axial stiffness drops by *75%* for a transverse displacement of *0.05*. This is a serious drawback of the double parallelogram flexure module. In the transition from a parallelogram flexure to a double parallelogram flexure, while geometric reversal improves the range of motion of the DOF and eliminates the purely kinematic errors along DOC, it proves to be detrimental to the quality of DOC.

Expressions similar to (28) have been derived previously using energy methods [11]. It has also been shown that the maximum axial stiffness can be achieved at any desired y location by tilting the beams of a double parallelogram flexure [15]. However, the rate at which stiffness drops with transverse displacements does not improve because even though beams of one module are tilted with respect to the beams of the other, they remain parallel within each module. Prior literature [16]

recommends the use of the double tilted-beam flexure, shown in Fig.10, over the double parallelogram flexure to avoid a loss in axial compliance resulting from a non-rigid secondary stage, but does not discuss the above-mentioned elastokinematic effect. To really eliminate this effect observed in the double parallelogram flexure, one needs to identify and address its basic source, which is the fact that the secondary stage is free to move transversely when an axial load is applied on the primary platform. Eliminating the translational DOF of the secondary stage should therefore resolve the current problem. In fact, it has been empirically suggested that an external geometric constraint be imposed, for example by means of a lever arm, on the secondary motion stage which requires it to have exactly half the transverse displacement of primary stage, when using a double parallelogram flexure [14]. However, this approach leads to design complexity in terms of practical implementation.

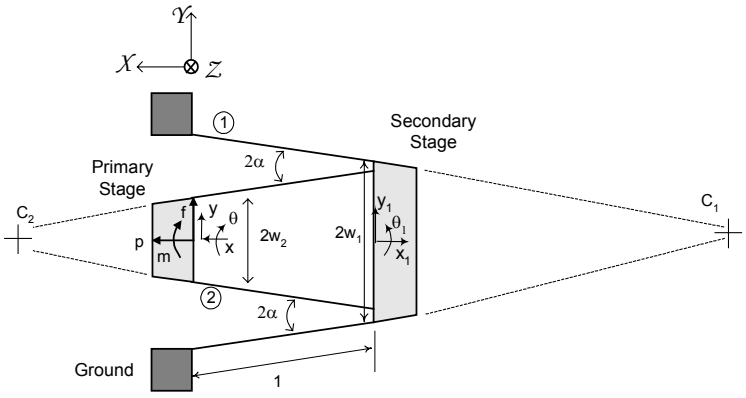

Fig.10 Double Tilted-beam Flexure

It is shown here that imposing a primary stage rotation in the double tilted-beam flexure can help suppress the DOF of the secondary stage. Referring to Fig.10, if the primary stage rotation θ is set to zero, for example, then results (21)-(23) lead to the following force-displacement relations.

$$\theta_1 \approx -\frac{y_1\alpha}{w_1} \;;\; \theta_2 \approx -\frac{y_2\alpha}{w_2} \;;\; y = y_1 + y_2 - \theta_1 \;;\; \theta = \theta_2 - \theta_1 \triangleq 0$$

$$\Rightarrow y_1 = \frac{w_1 y}{(w_1 + w_2 + \alpha)} \quad \text{and} \quad y_2 = \frac{w_2 y}{(w_1 + w_2 + \alpha)}$$

$$x \approx \frac{y^2}{2(\cos\alpha)^3 (w_1 + w_2 + \alpha)^2}\left[\left(-\bar{i}_1 w_1^2 + \bar{i}_2 w_2^2\right) + \left(\bar{r}_1 w_1^2 + \bar{r}_2 w_2^2\right) p\right] + \frac{p}{d(\cos\alpha)^2} \tag{29}$$

where y_1 and y_2 are the relative transverse displacements and $\bar{i}_1$, $\bar{i}_2$, $\bar{r}_1$, and $\bar{r}_2$ are as defined in expression (23) for modules 1 and 2, respectively. This derivation reveals that the additional elastokinematic term encountered in the double parallelogram flexure is suppressed in the double tilted-beam flexure. For typical dimensions (α*=0.1, t=1/60, w_1=0.5, w_2=0.3*), the axial stiffness drops by approximately *3%* over a transverse *y* displacement of *0.05*. This is a great improvement over the double parallelogram flexure in terms of the quality of DOC. It is also interesting to note that this flexure configuration does not entirely cancel the purely kinematic component of the axial displacement. Thus, an improvement in the stiffness along a DOC is achieved at the expense of the quality of DOF. Nevertheless, this configuration presents a good compromise between the desirable performance measures.

This mathematical result is amply supported by physical arguments. For a given *y* displacement, when a rotation constraint is imposed on the primary stage, the secondary stage has a virtual center of rotation located approximately at point C_1, owing to module 1, and a different virtual center of rotation located approximately at point C_2 due to module 2. Since, these two centers of rotation for the rigid secondary stage are spaced apart, the secondary stage is fully constrained, and the additional elastokinematic term encountered in the parallelogram flexure is eliminated. In the limiting case of α approaching zero, points C_1 and C_2 move out to infinity, and no longer pose conflicting constraints on the secondary stage, which therefore becomes free to translate in the transverse direction. This is the case of the double parallelogram flexure, for which it is not possible to constrain the secondary stage by imposing displacements on the primary stage because the transverse displacement and rotation of the constituent parallelograms are not kinematically related.

Of course, the effectiveness of the above strategy depends upon the effectiveness of the rotational constraint on the primary stage of the double tilted-beam flexure. Any mechanism that utilizes this module should be carefully designed to meet this requirement. Mirroring the design about the Y-axis, in Fig. 10, proves to be only partially successful because the resulting configuration does not entirely constrain the primary stage rotation. A hybrid design comprising of a double parallelogram flexure and a double-tilt beam flexure may work better because the former can provide the rotation constraint necessary for the latter to preserve the axial stiffness. Of course, this comes with a loss of symmetry, which influences the axial parasitic error motion, thermal and manufacturing sensitivity, among other performance measures. Once again, this discussion highlights the performance tradeoffs in flexure mechanism design.

CONCLUSION

Utilizing mathematical approximations, this paper presents simple closed-form expressions that accurately capture the force equilibrium related non-linearity in the beam flexure and its variations. These expressions are further employed to analyze several important flexure modules, and to qualitatively and quantitatively understand their force-displacement characteristics. The effects of shape variation, geometry variation, reversal and symmetry are analytically discussed. It has been shown by means of illustrative examples that there exist performance tradeoffs between the DOF and DOC of any flexure mechanism. In particular, the accuracy and axial

stiffness of approximate straight-line mechanisms are considered and ways to improve these are suggested.

If the transverse beam displacements are an order of magnitude less than the beam length, the proposed analysis has several advantages over the pseudo-rigid body methods. While the former provides closed-form and general relationships, the latter relies on model parameters that are load specific and have to been numerically calculated. More importantly, the pseudo-rigid body approximations do not adequately capture elastokinematic effects, which significantly affect the constraint properties of the beam and related flexures, as shown in this paper.

Finite Element Analysis has been performed to validate the closed-form analytical predictions. In all the cases, these two analysis methods match to within *10%* in terms of numerical values and almost exactly in terms of non-linear trends. However, the closed-form analysis allows quick calculations and parametric insights on flexure mechanism behavior, and therefore can potentially help in design conception and evaluation. Once a design with desirable performance attributes has been conceived, a final FEA can always be performed as a sanity check and to achieve higher prediction accuracy.

REFERENCES

1. Slocum, A.H., 1992, *Precision Machine Design*, Society of Manufacturing Engineers, Dearborn, MI.
2. Blanding, D.K., 1999, *Exact Constraint: Machine Design Using Kinematic Principles*, ASME Press, New York, NY.
3. Smith, S.T., 2000, *Flexures: Elements of Elastic Mechanisms*, Gordon and Breach Science Publishers, New York, NY.
4. Ejik, J.V., 1985, "On the Design of Plate Spring Mechanism", Ph.D. thesis, Delft University of Technology, Delft, The Netherlands.
5. Awtar, S., 2004, "Analysis and Synthesis of Planer Kinematic XY Mechanisms", Sc.D. thesis, Massachusetts Institute of Technology, Cambridge, MA. (http://web.mit.edu/shorya/www)
6. Bisshopp, K.E., and Drucker, D.C., 1945, "Large Deflection of Cantilever Beams", Quarterly of Applied Mathematics, **3**(3), pp. 272-275.
7. Frisch-Fay, R., 1963, *Flexible Bars*, Butterworth, Washington DC.
8. Mattiasson, K., 1981, "Numerical Results from Large Deflection Beam and Frame Problems Analyzed by Means of Elliptic Integrals", International Journal for Numerical Methods in Engineering, **17**, pp. 145-153.
9. Howell, L.L, 2001, *Compliant Mechanisms*, John Wiley & Sons, New York, NY.
10. Plainevaux, J.E., 1956, "Etude des deformations d'une lame de suspension elastique", Nuovo Cimento, **4**, pp. 922-928.
11. Legtenberg, R., Groeneveld, A.W. and Elwenspoek, M., 1996, "Comb-drive Actuators for Large Displacements", Journal of Micromechanics and Microengineering, **6**, pp. 320-329.
12. Haringx, J.A., "The Cross-Spring Pivot as a Constructional Element", Applied Science Research, **A1**(4), pp. 313-332.
13. Zelenika, S., and DeBona, F., 2002, "Analytical and Experimental Characterization of High Precision Flexural Pivots subjected to Lateral Loads", Precision Engineering, **26**, pp. 381-388.
14. Jones, R.V., 1988, *Instruments and Experiences: Papers on Measurement and Instrument Design*, John Wiley & Sons, New York, NY.
15. Zhou, G. and Dowd, P., 2003, "Tilted Folded-Beam Suspension for Extending the Stage Travel Range of Comb-drive Actuators", Journal of Micromechanics and Microengineering, **13**, pp. 178-183.
16. Saggere, L., Kota, S., 1994, "A New Design for Suspension of Linear Microactuators", ASME Journal of Dynamic Systems and Control, **55**(2), pp. 671-675.